Geodesy and Geodynamics 12 (2021) 451–458

Contents lists available at ScienceDirect

Geodesy and Geodynamics

journal homepage: http://www.keaipublishing.com/geog

Evaluation of global ocean tide models based on tidal gravity observations in China

Hongbo Tan [a, b, *], Olivier Francis [c], Guiju Wu [b], Guangliang Yang [b], Jiapei Wang [b], Xiaotong Zhang [b], Jinshui Huang [a], Chongyang Shen [b]

[a] School of Earth and Space Sciences, University of Science and Technology of China, Hefei, 230026, China
[b] Key Laboratory of Earthquake Geodesy, Institute of Seismology, China Earthquake Administration, Wuhan, 430071, China
[c] Faculty of Science, Technology and Communication, University of Luxembourg, Esch-sur-Alzette, L-4365, Luxembourg

ARTICLE INFO

Article history:
Received 19 January 2021
Accepted 2 August 2021
Available online 13 August 2021

Keywords:
Gravity signals
Ocean tidal loading
Global ocean tide models
gPhone gravimeter

ABSTRACT

Previous studies show that the calculated loading effects from global ocean tide models do not match actual measurements of gravity attraction and loading effects in Southeast Asia. In this paper, taking advantage of a unique network of gravity tidal stations all over the Chinese mainland, we compare the observed and modeled tidal loading effects on the basis of the most recent global ocean tide models. The results show that the average efficiencies of the ocean tidal loading correction for O_1, K_1, M_2 are 77%, 73% and 59%, respectively. The loading correction efficiencies using recent ocean tidal models are better than the 40 years old Schwiderskis model at coastal stations, but relative worse at stations far from ocean.

1. Introduction

Solid Earth is affected by tidal cycles triggered by the gravity attraction of the celestial bodies, in which the main contributions are from the Moon and Sun. The tides of the solid Earth, so-called body tides, are precisely modelled assuming that the Earth is an elastic body. However, about 70% of the Earth is covered with seawater which is also affected by tidal forces. Non-astronomical factors such as local depth of the water, ocean-floor topography, configuration of the coastlines, and other hydrographic and meteorological influences significantly complicate the ocean tides models. The periodic movements of seawater are responsible for gravity loading effects at the Earth's surface. These include direct effect (due to the direct gravity attraction of seawater mass) and indirect effect (due to the deformation of the Earth's crust caused by ocean load and the disturbed gravity field caused by the redistribution of the internal mass of the Earth) [1,2]. In the coastal areas, the ocean tidal loading (OTL) effects are more pronounced. The gravity loading can reach up to 10% of the earth tide, 90% for tilt, and 25% for strain. Even deep in the interior land, the effects can reach a few percent of the solid earth [1,3]. So, it is a non-negligible part in tidal analysis.

In the early 20th century in Europe, researchers found that the tidal factors between the South-to-North and West-to-East direction were inconsistent at one station, as well as the coastal and inland stations. At that time, they suspected it was caused by the influence of ocean tides [4]. In the 1960s, Munk [5] introduced the concept of the load Love numbers. With the improvement of Longman's [6] calculation method, 1000-order load Love numbers were calculated by Farrell [1]. The gravity, displacement, tilt and strain loading Green's functions were also computed that made possible to quantitatively study the ocean load. The first accurate and precise global ocean tidal model (OTM) was proposed by Schwiderski (SCHW) [7,8] based on the oceanic dynamic equation including a large number of tide gauge observations. Global OTL effects were computed by O. Francis [3] using the convolution method of Farrell [1]. With the development of satellite altimetry technology and the accumulation of data, a series of high precision and spatial resolution OTMs have been published, such as FES2014,

* Corresponding author. School of Earth and Space Sciences, University of Science and Technology of China, Hefei, 230026, China.
E-mail address: thbhong@163.com (H. Tan).

Peer review under responsibility of Institute of Seismology, China Earthquake Administration.

Production and Hosting by Elsevier on behalf of KeAi

https://doi.org/10.1016/j.geog.2021.08.001

DTU10, TPXO8, TPXO9, EOT11, HAMTIDE, NAO.99b [9–15]. The OTL precision depends on the OTM precision. Ocean tides are affected by the coastline configuration and submarine topography, especially in the bays, trenches and shallow sea. With the uncertainty of water depth, friction and viscosity coefficients at seafloor, the precision of the OTM in shallow water areas is still an issue [16]. Consequently, continental observations such as gravity and GPS are helpful to evaluate and even improve the OTMs [17].

Since 2007, a network of permanent relative gravity stations has been established in the framework of two projects: the Crustal Movement Observation Network of China (CMONOC) and the China Digital Earthquake Observation Network (CDEON) (see Fig. 1) [18]. Today, there are 78 stations with 84 gravimeters. More than 60 of them are equipped with gPhone or superconducting gravimeters (SG) with time sampling of 1Hz. The long time series provide precise and stable tidal data that offer the opportunity to validate, assess the precision or even improve OTMs. In this paper, tidal parameters of each station were extracted using the harmonic analysis method after a careful editing of the raw data. The efficiencies of OTL correction using different OTMs are compared and discussed to select reference OTMs for China.

2. Ocean loading modelling

The gravity acceleration due to the ocean tides direct attraction and loading is given by [1]:

$$I(\varphi,\lambda)=\rho_w\iint_{\Omega}G(\alpha)h(\varphi',\lambda')\mathrm{d}s' \tag{1}$$

where φ and λ denote latitude and longitude of the point of interest, ρ_w the mean density of seawater, Ω the domain of integration, $h(\varphi',\lambda')$ the elevation of the sea surface in-phase or in-quadrature for a given tidal wave on the surface area $\mathrm{d}s'$, and the angle α is calculated by

$$\cos\alpha=\sin\varphi\,\sin\varphi'+\cos\varphi\,\cos\varphi'\cos(\lambda-\lambda') \tag{2}$$

$G(\alpha)$ is the Green's Function expressed by

$$G(\alpha)=\frac{g}{m_e}\sum_{n=0}^{\infty}\left[n+2h_n'-n(n+1)k_n'\right]P_n(\cos\alpha) \tag{3}$$

in which g is the gravity acceleration, m_e the total mass of the Earth, h_n', k_n' the load Love numbers, and P_n the Legendre polynomials.

For the numerical evaluation, the ocean is usually divided into a set of cells, and the Green's function tabulated by Farrell [1] is interpolated for the intermediate values of α using cubic splines. Then the total response can be written as

$$I(\varphi,\lambda)=\rho_w\sum_{i=0}^{N}G(\alpha_i)h_i(\varphi',\lambda')\mathrm{d}s_i' \tag{4}$$

where N is the total number of oceanic cells of the OTM.

3. Gravity data and preprocessing

From more than 60 gravity stations, we selected 35 of them (Fig. 1). The others were not considered due to bad data quality, insufficient data or time stamps issues. All stations are equipped with gPhones or SGs with data length ranging from 1 to 3 years (Table 1). Most of the stations are located in the east and south of China (Fig. 1). Eleven stations are located along the ocean coasts. The closest station to the ocean is XiaMen (XM) station just less than 1 km to the nearest sea, while the farthermost station is ALeTai (ALT) at a distance of more than 2500 km.

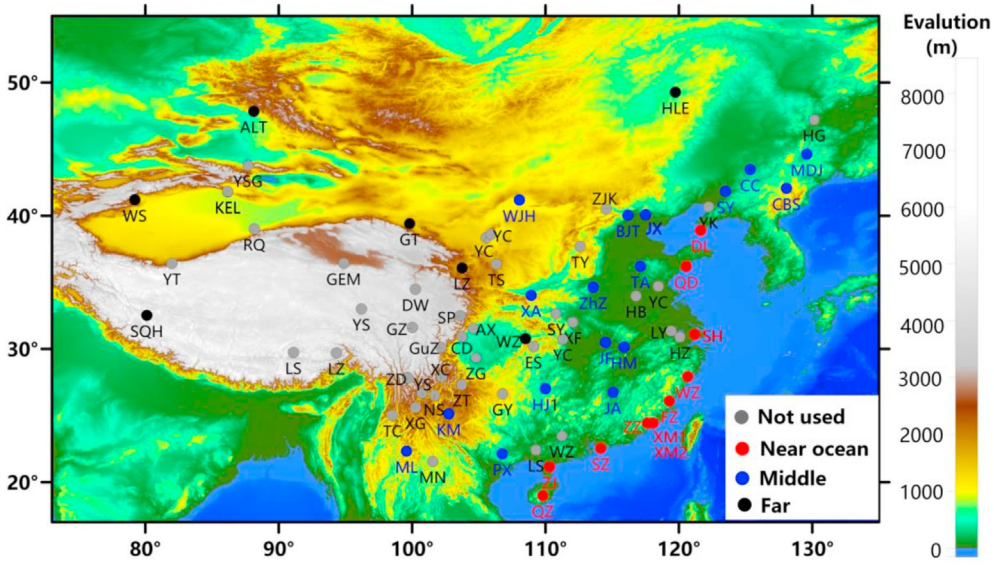

Fig. 1. Distribution of the stations of the China gravity network projected on the topographic surface. Red dots denote stations close to shorelines with distance $D \leq 60$ km. Blue dots denote stations with middle distance (60 km < $D \leq$ 1000 km) from oceans. Black dots represent stations with $D >$ 1000 km from oceans. Gray dots show stations which are discarded. QZ is the symbol for QiongZhong, so as ZJ: ZhanJiang, SZ: ShenZhen, ZZ: ZhangZhou, XM: XiaMen, FZ: FuZhou, WZ: WenZhou, SH: ShangHai, QD: QingDao, DL: DaLian, JX: Ji Xian, PX: Ping Xiang, CBS: Chang Bai Shan, BJT: Bai Jia Tuan, SY: Sheng Yang, TA: TaiAn, MDJ: MuDanJiang, CC: ChangChun, JA: JiAn, ZhZ: Zhen Zhou, HM: Huang Mei, HJ: Hong Jiang,KM: KunMing, ML: Meng Lian, JF: Jiu Feng, WJH: Wu Jia He, XA: XiAn, HLE: Hai La Er, WZ: Wan Zhou, LZ: LanZhou, SQH: Shi Quan He,GT: GaoTai, WS: WuShi, ALT: ALeTai.

Table 1
Length of the data series, atmospheric pressure admittance factor and precision of the gravity time series included in this paper.

No.	Station	Observation period (Year-Month-Day)	Atmospheric gravity admittance (10^{-8}m·s^{-2}/hPa)	Standard deviation of tidal parameters (10^{-8}m·s^{-2})
1	QZ	20090211–20130114	−0.364 ± 0.007	0.613
2	ZJ	20101203–20120229	−0.390 ± 0.038	1.772
3	SZ	20111103–20121103	−0.399 ± 0.014	0.657
4	ZZ	20091201–20130115	−0.290 ± 0.009	0.851
5	XM1	20101019–20111107	−0.331 ± 0.024	1.001
6	XM2	20101019–20120229	−0.298 ± 0.021	1.140
7	FZ	20150101–20161231	−0.229 ± 0.004	0.324
8	WZ	20150101–20161231	−0.360 ± 0.009	0.367
9	SH	20150101–20161231	−0.287 ± 0.009	0.806
10	QD	20101130–20120911	−0.303 ± 0.007	0.527
11	DL	20150101–20161231	−0.345 ± 0.003	0.328
12	JX	20110525–20120229	−0.324 ± 0.005	0.281
13	PX	20150101–20161231	−0.254 ± 0.004	0.267
14	CBS	20090310–20110416	−0.309 ± 0.006	0.575
15	BJT	20080101–20120411	−0.339 ± 0.002	0.293
16	SY	20100821–20120301	−0.363 ± 0.002	0.173
17	TA	20090201–20130114	−0.339 ± 0.002	0.351
18	MDJ	20090202–20130113	−0.346 ± 0.003	0.633
19	CC	20110526–20120229	−0.388 ± 0.005	0.280
20	JA	20110315–20120229	−0.305 ± 0.007	0.305
21	ZhZ	20080919–20130114	−0.337 ± 0.001	0.217
22	HM	20080930–20121231	−0.341 ± 0.002	0.455
23	HJ	20101019–20121008	−0.410 ± 0.006	0.481
24	KM	20111231–20130419	−0.323 ± 0.004	0.217
25	ML	20150101–20161231	−0.379 ± 0.003	0.216
26	JF	20090216–20111218	−0.324 ± 0.001	0.077
27	WJH	20090224–20130109	−0.302 ± 0.001	0.146
28	XA	20090316–20130115	−0.330 ± 0.002	0.127
29	HLE	20090101–20110308	−0.376 ± 0.002	0.255
30	WZ	20101107–20120101	−0.339 ± 0.006	0.317
31	LZ	20090219–20130115	−0.335 ± 0.001	0.188
32	SQH	20090917–20110530	−0.354 ± 0.001	0.082
33	GT	20090304–20111216	−0.381 ± 0.001	0.166
34	WS	20090131–20120812	−0.381 ± 0.002	0.309
35	ALT	20101029–20120229	−0.397 ± 0.004	0.180

We us Tsoft [19], a specifically designed software, for earth tide series pre-processing recommended by the International Center for Earth's Tides (ICET). An interactive remove-restore approach allows us editing the gravity data for gaps, steps and spikes on the 1-min sampling time series. The clean data are then decimated to hourly values using a low-pass digital filter. Those are finally used to estimate the observed tidal parameters with the Earth Tide Analysis and Prediction Program System ET34-X-V72 [20,21]. A band-pass filter is applied on the pre-processed hourly data to eliminate the instrumental drift. Then the diurnal, semi-diurnal and one-third-diurnal tidal constituents are separated according to the different characteristics of angular frequency of the tide.

4. Ocean loading correction

The periodic variation of seawater is considered as the synthetic result of the periodic motion of each tidal wave. So the tidal height $h(t)$ can be expressed as

$$h(t) = \sum_{i=1}^{N} A_i \cos(\omega_i t + \varphi_i) \tag{5}$$

where the tidal parameters of A_i, ω_i and φ_i are the amplitude, frequency and initial phase of the i^{th} tidal constituent. There are 11 major tidal constituents, including M_2, S_2, N_2, K_2, K_1, O_1, P_1, Q_1, M_f, M_m and S_{sa}. For each tidal constituent, we define $\boldsymbol{M}(M,0)$ as the vector of the modelled gravity solid Earth tide, $\boldsymbol{A}(A,\alpha)$ as the vector of the measured gravity tide, $\boldsymbol{L}(L,\lambda)$ as the OTL vector. The relationship between the first residual vector $\boldsymbol{B}(B,\beta)$ and the final residual vector $\boldsymbol{X}(X,\chi)$ after OTL correction are defined as (see Fig. 2):

$$\boldsymbol{X}(X,\chi) = \boldsymbol{B}(B,\beta) - \boldsymbol{L}(L,\lambda) \tag{6}$$

$$\boldsymbol{B}(B,\beta) = \boldsymbol{A}(A,\alpha) - \boldsymbol{M}(M,0) \tag{7}$$

where, $M, A, L, B, X$are the amplitudes, λ, χ, β are the phases of their corresponding vectors respectively. α is the phase lag between the observed gravity vector and the solid Earth Tide elastic model.

OTLs can be computed from Ocean Tide Loading Provider (http://holt.oso.chalmers.se/loading/) [22,23]. Amplitudes and phases of the 11 main constituents for more than 20 OTMs are offered from which vectors $\boldsymbol{B}$ and $\boldsymbol{X}$ are calculated.

5. Results

In this section, the results for all the 35 stations are presented. The stations are classified according to the distance from the nearest sea.

5.1. For all stations

Fig. 3a shows the Root-Mean-Squares (RMS) of the observational errors (M_0) for each station. It reflects the station environmental conditions (background noise, environmental change, …) and the data uncertainties. They vary between 0.08 and 1.77μgal (10^{-8}m/s^2). The average errors as a function of the distance from the sea are 0.76, 0.30 and 0.21 μgal for near, middle and far stations, respectively. Obviously, the observational errors of the 11 stations which are the closest to the sea are much bigger than the others. The total final gravity residuals were defined as

$$Tx = \sqrt{\sum_{i=1}^{N} X_i^2}, N = 8 \tag{8}$$

where X_i is the final residuals form equation (6) and i denotes one of the 8 major constituents (M_2, S_2, N_2, K_2, K_1, O_1, P_1, Q_1). It reflects the absolute efficiency of solid earth tide and OTL correction. The range of Tx is 0.14–3.45 μgal using the best OTM. The ratios between Tx and M_0 (Fig. 3b) indicate that there are still tidal signals

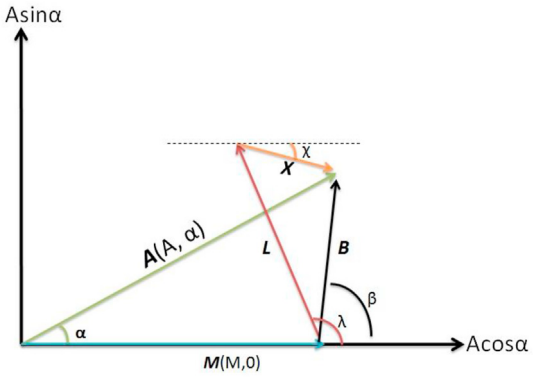

Fig. 2. The relation between observation, model and OTL vectors.

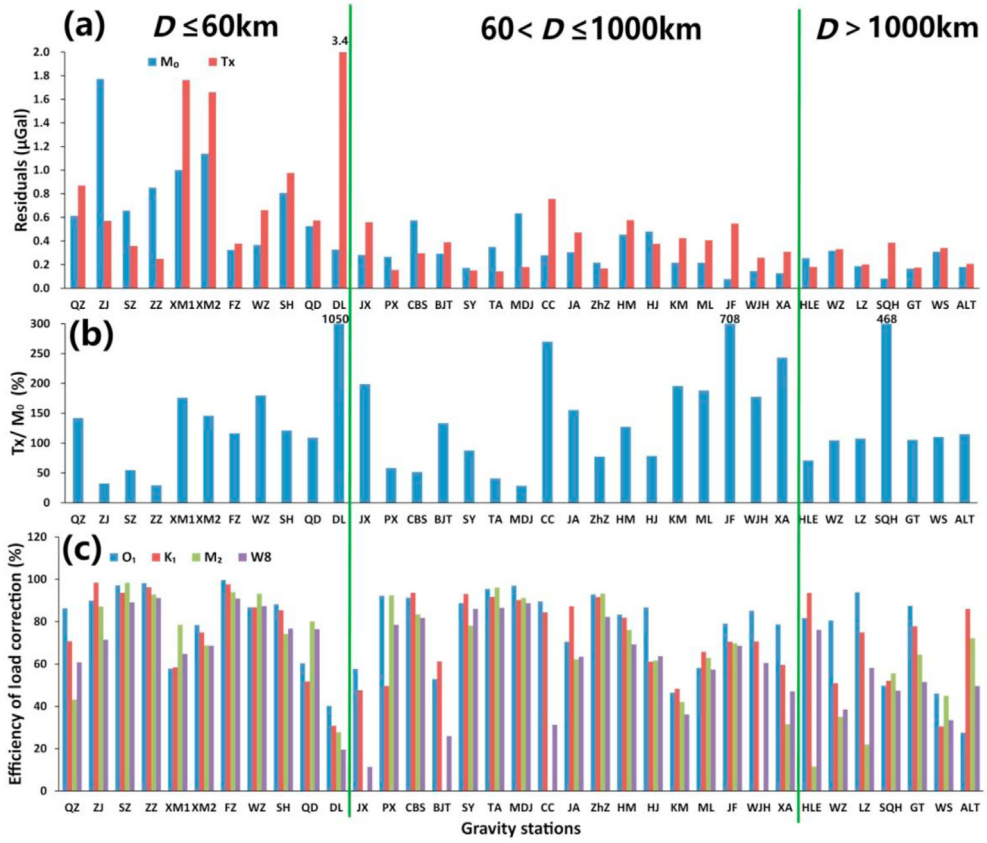

Fig. 3. Results of all gravity stations after OTL correction using the best ocean model: (a) observational RMS errors M_0 and total final residuals Tx; (b) ratios between Tx and RMS errors M_0; (c) efficiency of OTL correction defined by $(B-X)/B$. The order of the stations is depended on D, which denotes the distance from the station to the nearest ocean line.

in the residuals at a significant level: the leftover tidal signals are above the observational errors.24 of the 35 stations have a ratio higher than 100%. An extreme example is the DaLian (DL) station, for which the ratio is above 1000%. Fig. 3c also gives the relative efficiency of the OTL correction defined as *(B-X)/B* and

$$RE = \frac{\sqrt{\sum_{i=1}^{N} B_i^2} - \sqrt{\sum_{i=1}^{N} X_i^2}}{\sqrt{\sum_{i=1}^{N} B_i^2}}, \mathrm{N} = 8 \tag{9}$$

for O_1, K_1, M_2 and $W8$ (the 8 tidal constituents of M_2, S_2, N_2, K_2, K_1, O_1, P_1, Q_1). The average efficiency for O_1 is 77%, while 73%, 59% and 62% for K_1, M_2 and $W8$, respectively. So, O_1 shows the largest tides reduction compared to K_1 and M_2. More specifically, the OTL is ineffective at Ji Xian (JX), Bai Jia Tuan (BJT), ChangChun (CC), and Wu Jia He (WJH) stations.

The occurrence frequencies of the best OTM for each tidal constituent are plotted in Fig. 4a: 3 stations with two best OTMs for M_2, and 2 stations for $W8$. Overall, FES2014b provides the best corrections for O_1 at 12 stations, while SCHW provides the best for K_1, M_2 and $W8$ at 12, 8 and 9 stations. On the other hand, DTU10 performs well for W8. Interestingly, the gravity loadings obtained with SCHW are always different from the other models. In fact, the SCHW model is the best OTM for the Chinese mainland. The efficiency of OTL correction is displayed in Fig. 4b. There are 21 stations of which the correction efficiency reaches up to 80% for O_1 while

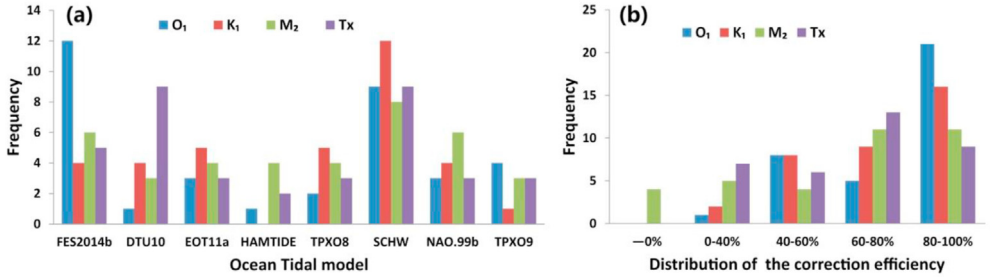

Fig. 4. Statistical results for all gravity stations: (a) the frequency of the best OTM; (b) the distribution of the correction efficiencies.

using the best OTM. The correction efficiencies are higher than 60% for K_1, M_2 and $W8$ at 25, 22 and 22 stations respectively.

5.2. Coastal stations

There are 11 stations close to the South and East China Sea with a distance less than 60 km. The observational errors (M_0) and total final residuals (Tx) are 0.32–1.77 and 0.25–3.45 μgal (Fig. 3a). Their ratios show that only 3 of them are less than 100%. The statistical results for the best OTM of the main ocean tides O_1, K_1, M_2 and W8 are displayed in Fig. 5a. There is not an obvious best OTM for the stations in coastal areas. DTU10 is the best OTM for K_1 and W8, while NAO.99b is the best on M_2. In summary, the DTU10, EOT11a and TPXO8 models perform slightly better than the others (see Fig. 5a). We see an efficiency of the OTL correction higher than 60% at most coastal stations. However, the total final residuals (Tx) are much bigger than the observational errors (for an example, $Tx = 3.4$ μgal and $M_0 = 0.33$ μgal at DaLian station). It indicates that there are still un-modeled OTL signals in the residuals.

5.3. Stations with middle distance from the ocean

17 stations are located at a distance between 60 and 1000 km from the ocean, including a superconducting gravimeter at Jiu Feng (JF) station. The observation errors (M_0) and total final residuals (Tx) are 0.077 and 0.55μgal, while the ranges for the other 16 stations are 0.13–0.63 and 0.14–0.76 μgal (Fig. 3a). Ratio is less than 100% for only 7 stations. The statistical results of the best OTM for the main ocean tides of O_1, K_1, M_2 and W8 are shown in Fig. 6a. At a middle distance, FES2014b is best on O_1, but obviously, SCHW is the best OTM. For most of the stations, the efficiencies of OTL correction are larger than 60%.

5.4. Stations far from ocean

There are 7 stations located far from the ocean at a minimum distance of 1000 km. The range of the observation errors (M_0) and total residuals (Tx) are 0.082–0.32 and 0.18–0.34 μgal (Fig. 3a). Their ratios show that only one of them is smaller than 100%. The statistical result in Fig. 7a shows that FES2014b and SCHW model

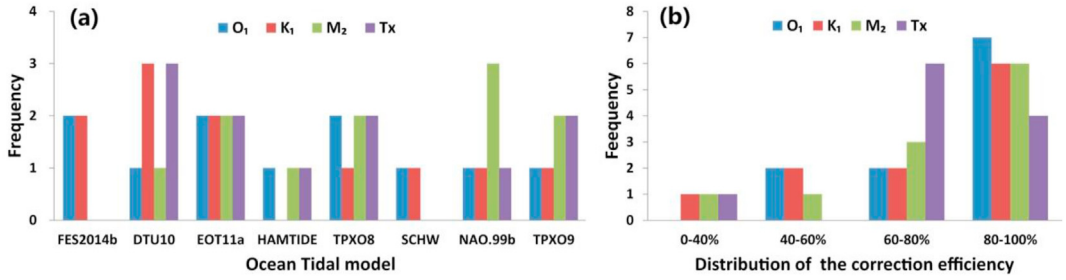

Fig. 5. Statistical results for near ocean stations (D ≤ 60 km): (a) the frequency of the best OTM; (b) the distribution of the correction efficiencies.

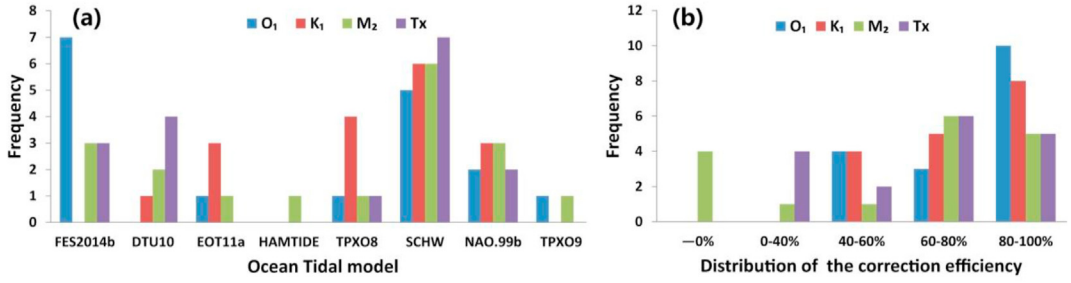

Fig. 6. Statistical results for middle distance stations (60 < D ≤ 1000 km): (a) the frequency of the best OTM; (b) the distribution of the correction efficiencies.

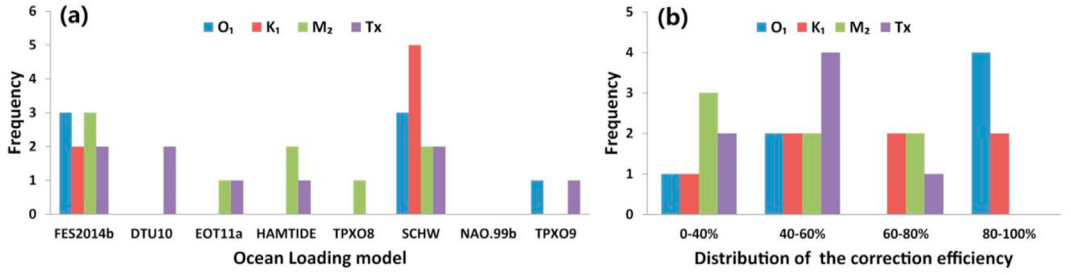

Fig. 7. Statistical results for far stations (D > 1000 km): (a) the frequency of the best OTM; (b) the distribution of the correction efficiencies.

are the best models. But the correction efficiency is worse than the near and middle stations from the seas. This could be attributed to the smaller signal-to-noise ratio.

6. Discussion

The distribution of the best OTM for O_1 is shown in Fig. 8a. The FES2014b is the best one for 12 stations, which are mainly located at the northeast and southeast of China. For the stations closer to the sea, EOT11a is the best OTM for the south coast stations. FES2014b is the best OTM in the east regions while SCHW is the best one in the north of Chinese coast. The situation is different for K_1: SCHW performs well at 12 stations with most of which located far from the ocean except DaLian (Fig. 8b). For M_2, SCHW is the best one at 8 stations, including the farthest station AaLe Tai, and 5 of them are located at southwest and north of China. Considering the main 8 tidal constituents, SCHW is the best for 9 stations with a distribution similar with M_2, and DTU10 is the best for 9 stations. Overall, it is not easy to decide which OTM performs the best. However, SCHW is generally better than the other OTMs except along the coastal areas. DTU10 is the next, and HAMTIDE performs the worst in China. The resolution of SCHW is $1^\circ \times 1^\circ$, and $1^\circ/8 \times 1^\circ/8$ for DTU10, $1^\circ/16 \times 1^\circ/16$ for FES2014b could explain why SCHW is less performing close to the sea. Although new models (such as FES2014, DTU10 and NAO.99b) use satellite altimetry, more accurate ocean bathymetry data and even a regional OTM around Japan, with higher resolution, they do not outclass SCHW at inland stations far from the coasts.

The final residuals X corrected with different OTMs are always similar to each other with differences less than 0.01 μgal. We cannot decide one OTM is better than all the others before without taking observational errors (E_{ob}) into account. Observational errors of each constituent are shown in Fig. 9. The average errors for O_1, K_1, M_2 and W8 for coastal stations are 0.027, 0.032, 0.043, 0.111 μgal, while 0.011, 0.015, 0.010, 0.045 μgal for middle range stations, and 0.009, 0.035, 0.009, 0.051 μgal for inland stations. There are only 4 stations where the ratios between the final residuals X and observational errors of each constituent are less than 200% (2 times of observational RMS) for O_1, and 4, 1, 3 stations for K_1, M_2, $W8$. It means that the efficiency of OTL correction is very low for most of the stations, especially at DaLian (DL), Jiu Feng (JF) and Shi Quan Hei (SQH) stations.

In order to consider the observational errors, we calculated the differences between the final residuals X and minimum X while using different OTMs. We only considered difference values higher than 2 times of the uncertainty. The results are shown in Fig. 10. They are different from those for which the observational errors are not taken into account. For coastal stations, SCHW is still the less performant OTM. DTU10, and EOT11a are generally the best OTMs. For the 8 main tidal constituents (W8), DTU10, EOT11a and NAO.99b are the best OTMs for the coastal stations in China. We cannot find a single best OTM for the regions further from the oceans. DTU10 is the best at 12 of the 17 stations based on W8 statistics. Further away, SCHW is the best model for O_1 and K_1, but worst when considering W8, while FES2014b is just the opposite.

Another factor that should be considered is the calibration of gravimeters. All the gravity meters have been calibrated by the manufacturer. The calibration factors were also controlled by comparison with the SGC0-053 at the Wuhan National Gravity and Earth Tide Observatory before deployment of the gPhones in China.

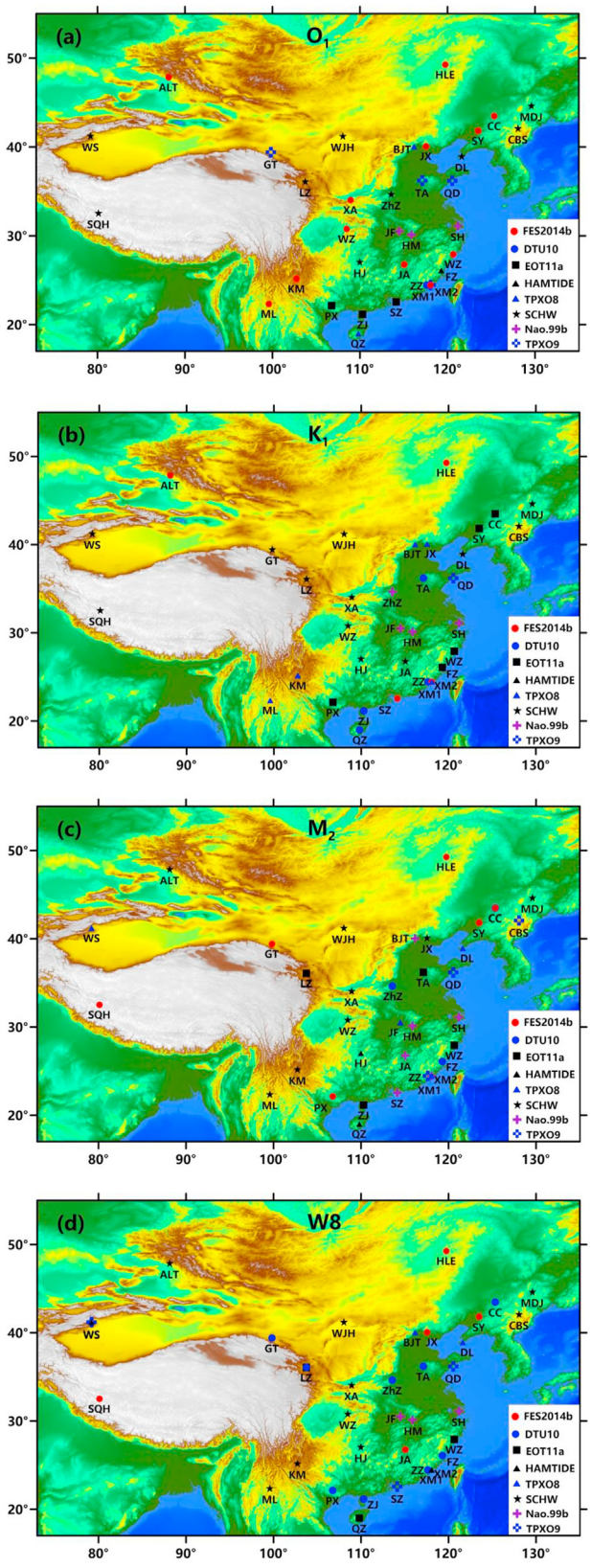

Fig. 8. The distribution of the best OTM: (a) for O_1; (b) for K_1; (c) for M_2; (d) for $W8$.

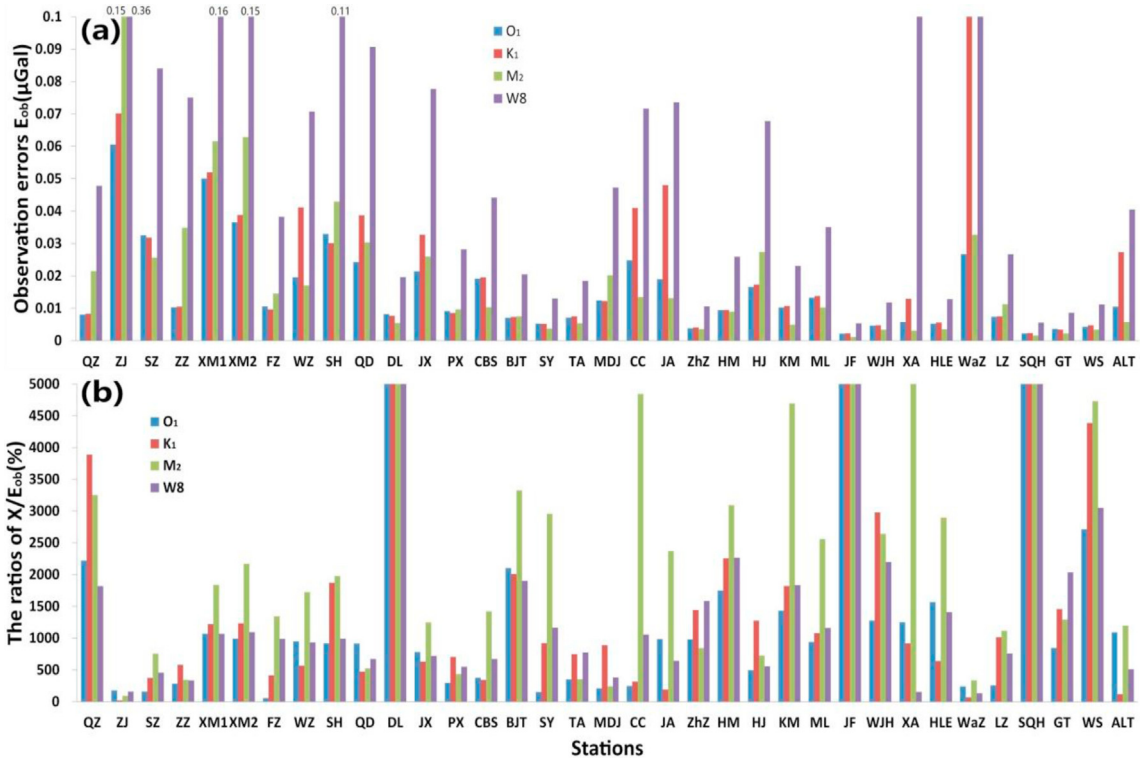

Fig. 9. Observational errors and the ratios of X/E_{ob} for each constituent.

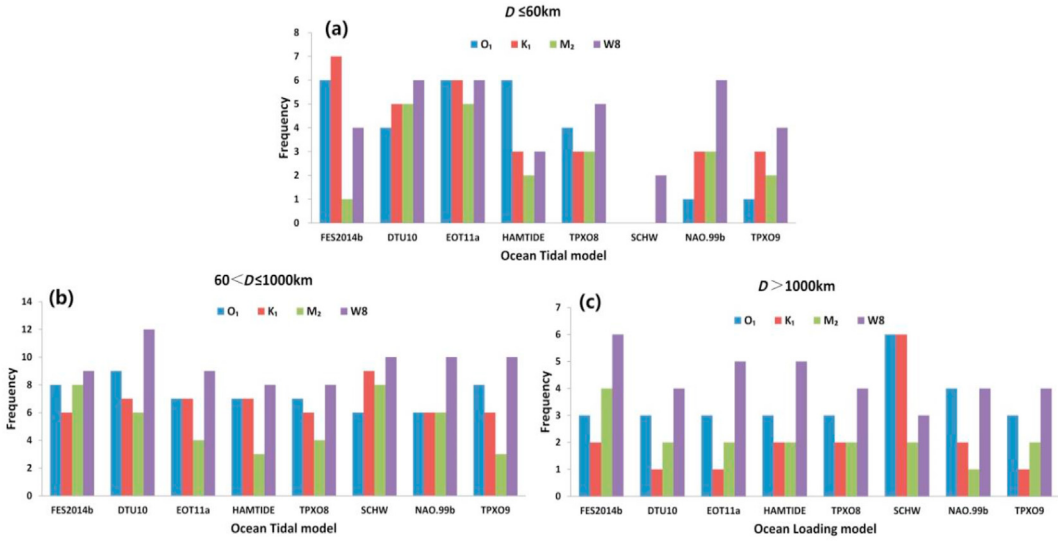

Fig. 10. Statistical results considering two times of observational RMS errors: a) for $D \leq 60$ km; b) for $60 < D \leq 1000$ km; c) for $D > 1000$ km.

Zhang Rui et al. [24] estimated the calibration factor of the gPhone-058 and found a value of 1.0084 ± 0.0009 × 10^{-8}ms^{-2}/mV. Its precision is a few orders of magnitude smaller than the Earth tides including the OTL.

7. Conclusions

During this last decade, China initiated an ambitious project of deploying a dense and homogenous tidal gravity network. Most of the stations are equipped with spring relative gPhone gravimeters. Only 2 stations are equipped with superconducting gravimeters. We use observations from 35 stations and carried out extensive comparisons between observed and calculated ocean tides attraction and loading effects for different OTMs. The outcome of these comparisons is mixed: none of the recent OTMs performs the best for all tidal constituents at every station. Surprisingly, the Schwiderski's model (SCHW), which has already been used for almost 40 years with a coarse resolution of 1° x 1°, is performing relative well with respect to the more recent OTMs. Similar results are obtained in Southeast Asia [25,26]. Dawei Li's [27] result also shows that

there is about 16 cm deviation between the global OTMs and Chinese tidal stations. It could be due to systematic errors of the OTM in the Chinese surrounding seas affecting the global OTMs. One way would be effective by inversing the ocean tides in the vicinity of China using gravity data.

Author contributions

All authors contributed to the study conception and design. Hongbo Tan completed the data processing, counting, analysis and the writing in the paper. Olivier Francis reviewed the paper, provided good suggestions and improved the language. Guiju Wu completed the data processing. Guangliang Yang calculated the OTL. Jiapei Wang analysed data. Xiaotong Zhang provided data and preliminary data processing. Jinshui Huang provided good suggestions. Chongyang Shen revised the abstract, conclusions and reviewed the paper. All authors read and approved the final manuscript.

Conflicts of interest

The authors declare that there is no conflicts of interest.

Acknowledgments

We are grateful to the Gravity and Deformation Sub center of China Earthquake Administration Data Sharing Center to provide the gravity data. We also thank to two anonymous reviewers for their comments that improved the manuscript. This research was funded by The National Natural Science Foundation of China (No. 41774015, 41704135 and U1939204) and National Key Research and Development Project of China (No. 2018YFE0206100, 2017YFC1500204).

References

[1] W.E. Farrell, Deformation of the Earth by surface loads, Rev. Geophys. Space Phys. 10 (3) (1972) 761–797.
[2] H.P. Sun, H.Z. Xu, S.C. Luo, J.Q. Xu, Study of the ocean models using tidal gravity observations, 1155-120, Acta Geod. Cartogr. Sinica 28 (2) (1999) (in Chinese).
[3] O. Francis, Global charts of ocean tide loading effects, J. Geophys.l Res. 95 (C7) (1990) 11411–11424.
[4] Q.P. Wu, Gravity and Earth Tide, Seismological Press, Beijing, China, 1997 (in Chinese).
[5] W. Munkand, D.E. Cartwright, Tidal spectroscopy and prediction, Philos. Trans. R. Soc. London, Ser. A 259 (1966) 533–581.
[6] I.M. Longmen, A Green's function for determining the deformation of the Earth under surface mass loads : 2 Computation and numerical results, J. Geophys. Res. 68 (1963) 485–498.
[7] E.W. Schwiderski, Ocean tides. Part I: global ocean tidal equations, Mar. Geodes. 3 (1980) 161–217.
[8] E.W. Schwiderski, Ocean tides. Part II: a hydrodynamical interpolation model, Mar. Geodes. 3 (1980) 219–255.
[9] F. Lyard, F. Lefevre, T. Letellier, O. Francis, Modelling the global ocean tides: modern insights from FES2004, Ocean Dynam. 56 (2006) 394–415, https://doi.org/10.1007/s10236-006-0086-x.
[10] L. Carrere, F. Lyard, M. Cancet, A. Guillot, N. Picot, Finite Element Solution FES2014, a New Tidal Model - Validation Results and Perspectives for Improvements, presentation to ESA Living Planet Conference, 2016. Prague.
[11] Y. Cheng, O.B. Andersen, Improvement in global ocean tide model in shallow water regions, OSTST, Lisbon, Poster SV 1–68 (2010) 18–22.
[12] G.D. Egbert, S.Y. Erofeeva, Efficient inverse modeling of barotropic ocean tides, J. Atmos. Ocean. Technol. 19 (2) (2002) 183–204, https://doi.org/10.1175/1520-0426(2002)019<0183:EIMOBO>2.0.CO, 2.
[13] R. Savcenko, W. Bosch, EOT11a - a new tide model from Multi-Mission Altimetry, October, OSTST Meeting (2011) 19–21 (San Diego).
[14] E. Taguchi, D. Stammer, W. Zahel, Inferring deep ocean tidal energy dissipation from the global high-resolution data-assimilative HAMTIDE model, J. Geophys. Res. 119 (C7) (2014) 4574–4592, https://doi.org/10.1002/2013JC009766.
[15] K. Matsumoto, T. Takanezawa, M. Ooe, ocean tide models developed by assimilating TOPEX/POSEIDON altimeter data into hydrodynamical model: a global model and a regional model around Japan, J. Oceanogr. 56 (2000) 567–581.
[16] C.K. Shum, P. L Woodworth, O.B. Andersen, G.D. Egbert, O. Francis, C. King, S.M. Klosko, C. Le Provost, X. Li, J.M. Molines, M.E. Parke, R.D. Ray, M.G. Schlax, D. Stammer, C.C. Tierney, P. Vincent, C.I. Wunsch, Accuracy assessment of recent ocean tide models, J. Geophys. Res. 102 (C11) (1997) 25173–25194, https://doi.org/10.1029/97JC00445.
[17] G.H. Fang, Y.K. Kwok, K. Yu, Y.H. Zhu, Numerical simulation of principal tidal constituents in the south China sea, Gulf of Tonkin and Gulf of Thailand, Continent. Shelf Res. 19 (7) (1999) 845–869.
[18] X.T. Zhang, Y. Jiang, K. Zhang, X.L. Zhang, The influence of observation environment on background noise level of gPhonegravimeter, Geodesy Geodynam. 8 (6) (2017) 443–447, https://doi.org/10.1016/j.geog.2017.06.002.
[19] P. Vauterin, Tsoft: graphical and interactive software for the analysis of Earth tide data, in: Proc. 13th Int. Sympos. On Earth Tides, Brussels, Observatoire Royal de Belgique, Serie Geophysique, 1998, pp. 481–486.
[20] H.G. Wenzel, The nanogal software: earth tide data preprocessing package ETERNA3.30, Bull. Inf. Marées Terrestres 124 (1996) 9425–9439.
[21] K. Schueller, User's Guide. Manual-02-ET34-ANA-V71, Surin, 2019.
[22] M.S. Bos, H.G. Scherneck, Computation of Green's functions for ocean tide loading, in: G. Xu (Ed.), Sciences of Geodesy –ii, Springer Berlin Heidelberg, 2013, pp. 1–52.
[23] H.G. Scherneck, A parametrized solid Earth tide mode and ocean loading effects for global geodetic base-line measurements, Geophys. J. Int. 106 (3) (1991) 677–694, 1991.
[24] R. Zhang, J. Wei, Z.W. Liu, H. Li, H.T. Hao, gPh058 gravimeter by use of observations with SGC053 superconducting gravimeter, J. Geodesy Geodyn. 31 (5) (2011) 151–155 (in Chinese).
[25] P. Melchior, O. Francis, B. Ducarme, Tidal gravity measurements in Southeast Asia, Marees Terr. Bull. Inf. 125 (1996) 9493–9507.
[26] O. Francis, T. van Dam, Tidal gravity measurements in Southeast Asia revisted, Prog. Geodesy Geodyn. (2014) 338–342. http://orbilu.uni.lu/handle/10993/16440.
[27] D.W. Li, J.C. Li, T.Y. Jin, M.Z. Hu, Accuracy estimation of recent global ocean tide models using tide gauge data, J. Geodesy Geodyn. 32 (4) (2012) 106–110 (in Chinese).

Hongbo Tan, is a PhD student at the University of Science and Technology of China and an associate researcher at the Institute of Seismology, China Earthquake Administration. His research interests include gravity observation, earth tide and seismic dislocation.